Heart

Cardiac Alpha-V Beta-3 Integrin Expression Following Acute Myocardial Infarction in Humans

Journal:	*Heart*
Manuscript ID	heartjnl-2016-310115.R2
Article Type:	Original research article
Date Submitted by the Author:	16-Sep-2016
Complete List of Authors:	Jenkins, William; University of Edinburgh, Department of Cardiovascular Sciences; Mayo Clinic, Department of Cardiovascular Diseases Vesey, Alex; University of Edinburgh, Department of Cardiovascular Sciences Stirrat, Colin; University of Edinburgh, Department of Cardiovascular Sciences Connell, Martin; University of Edinburgh Lucatelli, Christophe; University of Edinburgh, Clinical Research Imaging Centre Neale, Anoushka; University of Edinburgh, Department of Cardiovascular Sciences Moles, Catriona; University of Edinburgh, Department of Cardiovascular Sciences Vickers, Anna; University of Edinburgh, Department of Cardiovascular Sciences Fletcher, Alison; University of Edinburgh, Clinical Research Imaging Centre Pawade, Tania; University of Edinburgh, Department of Cardiovascular Sciences Wilson, Ian; Edinburgh Molecular Imaging Ltd Rudd, James; University of Cambridge, Division of Cardiovascular Medicine van Beek, Edwin; University of Edinburgh, Clinical Research Imaging Centre Mirsadraee, Saeed; University of Edinburgh, Clinical Research Imaging Centre Dweck, Marc; University of Edinburgh, Centre for Cardiovascular Sciences Newby, David; University of Edinburgh, Centre for Cardiovascular Sciences
Keywords:	Positron emission tomographic (PET) imaging < Cardiac imaging and diagnostics < CARDIAC PROCEDURES AND THERAPY, Acute myocardial infarction < Coronary artery disease < DISEASES, Cardiac magnetic resonance (CMR) imaging < Cardiac imaging and diagnostics < CARDIAC PROCEDURES AND THERAPY, Advanced cardiac imaging < Cardiac imaging and diagnostics < CARDIAC PROCEDURES AND THERAPY
Abstract:	Objective Maladaptive repair contributes towards the development of heart failure following myocardial infarction (MI). The $\alpha v \beta 3$ integrin receptor is a key

mediator and determinant of cardiac repair. We aimed to establish whether αvβ3 integrin expression determines myocardial recovery following MI.

Methods

18F-Fluciclatide (a novel αvβ3-selective radiotracer) positron emission tomography (PET) and computed tomography (CT) imaging, and gadolinium-enhanced magnetic resonance imaging (CMR) were performed in 21 patients 2-weeks after ST-segment elevation MI (anterior,n=16; lateral,n=4; inferior,n=1). Cardiac CMR was repeated 9 months after MI. Seven stable patients with chronic total occlusion (CTO) of a major coronary vessel, and 9 healthy volunteers underwent a single PET/CT and CMR.

Results

18F-Fluciclatide uptake was increased at sites of acute infarction compared to remote myocardium (tissue-to-background ratio (TBRmean) 1.34±0.22 vs 0.85±0.17; p<0.001) and myocardium of healthy volunteers (TBRmean 1.34±0.22 vs 0.70±0.03; p<0.001). There was no 18F-fluciclatide uptake at sites of established prior infarction in CTO patients, with activity similar to the myocardium of healthy volunteers (TBRmean 0.71±0.06 vs. 0.70±0.03, p=0.83). 18F-Fluciclatide uptake occurred at sites of regional wall hypokinesia (wall motion index ≥1 vs 0; TBRmean 0.93±0.31 vs 0.80±0.26 respectively, p<0.001) and subendocardial infarction. Importantly, although there was no correlation with infarct size (r=0.03, p=0.90) or inflammation (C-reactive protein, r=-0.20, p=0.38), 18F-fluciclatide uptake was increased in segments displaying functional recovery (TBRmean 0.95±0.33 vs 0.81±0.27, p=0.002) and associated with increase in probability of regional recovery.

Conclusions

18F-Fluciclatide uptake is increased at sites of recent MI acting as a biomarker of cardiac repair and predicting regions of recovery.

Cardiac Alpha-V Beta-3 Integrin Expression Following Acute Myocardial Infarction in Humans

William SA Jenkins, MBChB [1,5]

Alex T Vesey, MBChB [1]

Colin Stirrat MBChB [1]

Martin Connell, PhD [2]

Christophe Lucatelli PhD [2]

Anoushka Neale [1]

Catriona Moles [1]

Anna Vickers MBChB [1]

Alison Fletcher PhD [2]

Tania Pawade MBChB [1]

Ian Wilson PhD [4]

James HF Rudd MBChB, PhD [3]

Edwin JR van Beek MD, PhD [2]

Saeed Mirsadraee MD, PhD [2]

* Marc R Dweck MBChB, PhD [1]

* David E Newby MBChB, PhD [1]

[1] Department of Cardiovascular Sciences, University of Edinburgh, Edinburgh

[2] Clinical Research Imaging Center, University of Edinburgh, Edinburgh

[3] Division of Cardiovascular Medicine, University of Cambridge, Cambridge

[4] Edinburgh Molecular Imaging Ltd, Edinburgh

[5] Department of Cardiovascular Diseases, Mayo Clinic, Rochester, Minnesota

*Contributed equally

Corresponding Author

Dr William SA Jenkins, BSc. MBChB. MRCP

Cardiology Research Fellow

Department of Cardiovascular Sciences, Chancellors Building, 49 Little

France Crescent, University of Edinburgh, EH16 4SB.

Telephone 0131-242-6515

Fax: 0131-242-6379

Email; williamjenkins@doctors.net.uk

Word count; 3,093

1
2
3
4
5
6
7
8
9
10
...

Abstract

Objective

Maladaptive repair contributes towards the development of heart failure following myocardial infarction (MI). The $\alpha_v\beta_3$ integrin receptor is a key mediator and determinant of cardiac repair. We aimed to establish whether $\alpha_v\beta_3$ integrin expression determines myocardial recovery following MI.

Methods

18F-Fluciclatide (a novel $\alpha_v\beta_3$-selective radiotracer) positron emission tomography (PET) and computed tomography (CT) imaging, and gadolinium-enhanced magnetic resonance imaging (CMR) were performed in 21 patients 2 weeks after ST-segment elevation MI (anterior,n=16; lateral,n=4; inferior,n=1). Cardiac CMR was repeated 9 months after MI. Seven stable patients with chronic total occlusion (CTO) of a major coronary vessel, and 9 healthy volunteers underwent a single PET/CT and CMR.

Results

18F-Fluciclatide uptake was increased at sites of acute infarction compared to remote myocardium (tissue-to-background ratio (TBR$_{mean}$) 1.34±0.22 vs 0.85±0.17; p<0.001) and myocardium of healthy volunteers (TBR$_{mean}$ 1.34±0.22 vs 0.70±0.03; p<0.001). There was no 18F-fluciclatide uptake at sites of established prior infarction in CTO patients, with activity similar to the myocardium of healthy volunteers (TBR$_{mean}$ 0.71±0.06 vs. 0.70±0.03, p=0.83). 18F-Fluciclatide uptake occurred at sites of regional wall hypokinesia (wall motion index ≥1 vs 0; TBR$_{mean}$ 0.93±0.31 vs 0.80±0.26 respectively, p<0.001) and subendocardial infarction. Importantly, although there was no correlation

with infarct size (r=0.03, p=0.90) or inflammation (C-reactive protein, r=-0.20,

p=0.38), 18F-fluciclatide uptake was increased in segments displaying

functional recovery (TBR_{mean} 0.95±0.33 vs 0.81±0.27, p=0.002) and

associated with increase in probability of regional recovery.

Conclusions

18F-Fluciclatide uptake is increased at sites of recent MI acting as a

biomarker of cardiac repair and predicting regions of recovery.

Key Questions

What is already known about this subject?

Non-invasive imaging of myocardial remodeling may permit understanding, prediction and potential modification of adverse remodeling and the syndrome of delayed heart failure following MI. The $\alpha_v\beta_3$ integrin cell surface receptor is intrinsic to angiogenesis, inflammation and fibrogenesis in remodeling myocardium and has been targeted using positron emission tomography (PET) radiotracers in murine and small human studies following MI. However, the role of $\alpha_v\beta_3$ integrin radiotracers in humans following MI is incompletely defined.

What does this study add?

Using PET imaging with kinetic analysis, computed tomography (CT) contrast angiography and cardiac magnetic resonance imaging we have demonstrated 18F-fluciclatide binding with $\alpha_v\beta_3$ integrin receptors in regions of acute myocardial infarction and in the remote myocardium. 18F-fluciclatide uptake correlates with functional impairment and may predict myocardial recovery.

How might this impact on clinical practice?

Our study fulfils a key step validating $\alpha_v\beta_3$ integrin receptor imaging in humans following MI. This novel characterisation of myocardial remodeling may hold potential as a biological end-point in the study of novel therapies following MI.

Introduction

Ischemic heart disease remains the leading cause of death globally, with over 1 million people suffering acute myocardial infarction (MI) per year in the USA alone. As the acute management of MI improves, the number of patients surviving acute myocardial injury is higher than ever before. In this population, adverse cardiac remodeling and the syndrome of delayed heart failure represents a major cause of morbidity.[1] Understanding reparative mechanisms following infarction is becoming increasingly important.

Repair following MI is triggered by a complex interaction of neurohormonal activation and up-regulation of angiogenic and pro-fibrotic transcription factors that initiate the restoration of a capillary network through angiogenesis and re-endothelialization, as well as extracellular matrix (ECM) remodeling through macrophage accumulation and fibroblast activation. This interplay of angiogenesis, inflammation and fibrosis determines the extent of preservation and restoration of myocardial integrity.[2] In some circumstances, maladaptive persistent processes may encourage remodeling and scarring to extend into the myocardium long after the initial causative injury. This may lead to progressive ventricular dilatation, ventricular dysfunction and heart failure.

The $\alpha_v\beta_3$ integrin is a trans-membrane cell surface receptor that facilitates migration, proliferation and interaction with the ECM, thereby allowing cells to respond to, and in turn modify, their extracellular environment. Expressed at low levels by quiescent endothelial cells, $\alpha_v\beta_3$ integrin is markedly up

regulated in states of angiogenesis within the myocardium after infarction.[3,4]

In addition, pre-clinical and clinical studies document $\alpha_v\beta_3$ integrin expression

by both activated cardiac myofibroblasts and macrophages during

margination and chemotaxis. Thus, $\alpha_v\beta_3$ integrin expression appears central to

the co-ordination of repair following MI.

In this study, we investigated the expression of $\alpha_v\beta_3$ integrin following MI using

the novel $\alpha_v\beta_3$ integrin-selective radiotracer, 18F-fluciclatide, combined with

cardiac positron emission tomography (PET), computed tomography (CT) and

cardiovascular magnetic resonance (CMR). The study aims were to describe

and characterize the uptake of this radiotracer, and to correlate it with clinical

markers of disease severity and functional recovery in patients with recent MI.

Methods

PET/CT scanning with 18F-fluciclatide and CMR were performed in 3 groups of participants recruited from Royal Infirmary of Edinburgh between July, 2013, and February, 2015. Exclusion criteria were age <40 years, women of childbearing potential not taking contraception, severe renal failure (serum creatinine >2.8 mg/dL) or hepatic failure (Childs-Pugh grade B or C), atrial fibrillation, contrast allergy, inability to undergo scanning and inability to provide informed consent. Studies were performed with approval of the local research ethics committee, in accordance with the Declaration of Helsinki, and with the written informed consent of each participant.

Study Participants

Acute MI group. Patients with recent acute ST-segment elevation MI and peak high-sensitivity cardiac troponin I (hs-cTnI) >10,000 ng/L were invited to attend for PET/CT with 18F-fluciclatide 14±7 days after their initial presentation. CMR was performed within 7 days of PET/CT scanning. Patients were then invited to return for a second PET/CT with 18F-fluciclatide 10 weeks after MI and for a follow-up CMR at 9 months.

Chronic Total Occlusion (CTO) group. Patients with an angiographically-documented complete occlusion of a major epicardial artery and stable cardiac symptoms for >6 months were invited to attend for a single PET/CT with 18F-fluciclatide and CMR.

Control group. Volunteers with normal left ventricular systolic function, no structural heart disease, and no symptoms of heart failure or MI underwent a single PET/CT with 18F-fluciclatide and CMR.

Histology Cohort

For histological analysis, myocardial biopsy samples were obtained from patients undergoing coronary artery bypass grafting following recent MI. Patients with large ST-elevation MI (<14 days, hs-cTnI >10,000 ng/L) were considered for inclusion forming a separate cohort from the acute MI group.

Radiosynthesis of 18F-Fluciclatide

The radiotracer was manufactured at the Clinical Research Imaging Centre, University of Edinburgh on an automated module (FASTlab synthesizer; GE Healthcare) by coupling an amino-oxy-functionalized peptide precursor (AH111695) with 4-18F-fluorobenzaldehyde at pH 3.5 to form 18F-fluciclatide. Full description of this synthesis has been published.[5-7]

Imaging Assessments

All patients underwent PET-CT imaging of the thorax with a hybrid scanner (Biograph mCT, Siemens Medical Systems, Germany) after administration of a target dose of 230 MBq 18F-fluciclatide (Supplementary Material). No dietary restrictions were required prior to radiotracer administration. Attenuation-correction CT scanning (non-enhanced 120 kV and 50 mA, 3-mm slices) was performed, followed by PET acquisition with electrocardiographic (ECG) gating. To assess tracer pharmacodynamics and the optimum timing of scanning, dynamic thoracic PET imaging was initially performed in 10 subjects in 3-dimensional mode with a single bed position for 70 min. The

remainder of study subjects underwent static imaging performed at the optimal time point as determined from the dynamic studies (40-min post-injection) using a single 30-min bed position in list mode. Immediately after PET acquisition cardiac CT angiography was performed on the hybrid scanner (Supplementary Material).

PET Reconstruction and Analysis

Kinetic analysis of the dynamic scans was undertaken to investigate 18F-fluciclatide uptake within the myocardium (Supplementary Material). For all patients, static ECG-gated PET images were reconstructed in diastole, 40-70 min post-injection. Myocardial 18F-fluciclatide uptake was assessed by an experienced observer (WJ) by drawing regions of interest (ROI) in each myocardial segment using the standardized 16-segment approach [8]. Additionally, ROI's were drawn in focal regions affected by infarction and in regions of remote myocardium. This was achieved using the fused CT angiography and CMR images as a reference, and with care taken to avoid contamination from the blood-pool signal. PET data were corrected for residual blood pool activity (standard uptake value, SUV) in the superior vena cava and expressed as a mean tissue-to-background ratio (TBR_{mean}). SUV_{max} and TBR_{max} values were also calculated alongside the corrected SUV (SUV_C) values, where blood pool activity was subtracted from myocardial uptake (Supplementary Material).

CMR Imaging

Cardiac CMR with assessment of late gadolinium enhancement (LGE) and T1 mapping was performed at 3T (MAGNETOM Verio, Siemens AG, Healthcare

Sector, Germany) with calculation of left ventricular function, wall motion index (WMI), transmurality of LGE, and extracellular volume fraction (ECV, Supplementary Material).

Histology

Briefly, a core cardiac biopsy was taken from the peri-infarct zone, fresh frozen and sectioned in cryosection medium (Supplementary Material). Adjacent tissue sections were stained with hematoxylin-eosin (HE) for conventional, smooth muscle actin, CD31, CD68 (clone PG-M1), and integrin $\alpha_v\beta_3$ antibody clone LM609 (Millipore) before digital imaging (Axioscan.Z1, Zeiss, UK) and histopathological examination

Statistical Analysis

We explored myocardial radiotracer uptake in 3 groups of patients, comparing them to CMR and clinical indices of cardiac function. Continuous data were tested for normality with the D'Agostino and Pearson Omnibus test. Continuous normal variables were expressed as mean±standard deviation and compared using Students t-testing or analysis of variance (ANOVA) testing when comparing more than 2 groups. Continuous non-normal variables were presented as median [interquartile range] and compared using the Mann-Whitney or Kruskal-Wallis test when evaluating two/more than two groups. Interobserver reproducibility was calculated by Bland-Altman method and presented as mean bias ±2 standard deviations, and intraclass correlation coefficients (ICC) with 95% confidence intervals (CI). The chi-squared test was used for analysis of categorical variables. Univariable and multivariable logistic regression models were used to determine factors

associated with an improvement in segmental myocardial function. Statistical

analysis was performed with GraphPad Prism version 6 (GraphPad Software

Inc., USA) and JMP version 10.0 (SAS Software, North Carolina, USA) where

appropriate. A two-sided P-value<0.05 was considered statistically significant.

Results

Thirty-seven subjects underwent PET/CT after injection of 229±12 MBq 18F-fluciclatide: 21 patients with acute MI, 7 patients in the CTO group and 9 healthy volunteers (Tables 1 and 2). The groups were generally well balanced for age, sex and body-mass index. Healthy subjects had a lower prevalence of cardiovascular risk factors (Table 1). The mean radiation dose per participant for those who received a single PET/CT imaging assessment was 13.6 (range 7.8-18.9) mSv, and 21.9 (range 16.5-28.7) mSv in those who underwent repeat PET scanning.

CMR Characterisation of Myocardial Infarction & Remodeling

There were no areas of infarction in control subjects. All patients within the acute MI cohort (n=21) had visible infarction on CMR 13±5 days after MI. These infarcts were large (infarct size 12±7 g/m^2, peak cardiac troponin I 50,000 [26,753-50,000] ng/L) and featured the anterior (n=16) and lateral (n=4) territories predominantly, while 1 patient had an inferior MI. All subjects received emergency coronary angiography with successful revascularization 197 [148-342] min from the onset of symptoms (Table S1).

Old infarcts were present in 6 of 7 patients in the CTO group. Although there was no difference in infarct size [g/m^2] between MI and CTO groups (p=0.34), the left ventricular ejection fraction (LVEF) was reduced with a larger WMI score in those with recent MI (p<0.01 compared to either the CTO or control group, Table 2).

Seventeen patients from the acute MI group received follow-up CMR imaging 287±37 days after MI. During this timeframe, there were improvements in LVEF (p<0.01) and regional wall motion (WMI; p<0.005). In total, 43 of 272 myocardial segments (16%) showed an improvement in regional wall motion, while 226 segments remained unchanged and 3 segments displayed functional deterioration. Infarct size and LV mass also improved (p=0.03 and p<0.01 respectively, Table 3).

Histology & Dynamic Myocardial 18F-Fluciclatide PET

In an exploratory analysis, 2 patients scheduled for coronary artery bypass surgery within 14 days of infarction underwent myocardial biopsies from the peri-infarct zone (Figure 1). This showed predominantly viable myocardium with widespread positive staining for $\alpha_v\beta_3$ integrin, largely in regions that co-localized to CD31-positive vascular endothelial cells. Interestingly, these sites represented mainly angiogenic microvasculature, although there was scattered co-localisation with dual smooth muscle actin- and CD31-positive arterioles. There were lesser numbers of CD68-positive inflammatory cells and smooth muscle actin-positive myofibroblasts, but where present, they also co-registered with $\alpha_v\beta_3$ integrin expression (Figure 1).

Dynamic PET studies were performed in a subgroup of 10 patients. 18F-Fluciclatide activity within the region of myocardial infarction increased gradually and reached a plateau at around 30-40 min (Figure 2). The injected activity was cleared from the blood pool with a half-life of about 10 min, so that it remained relatively high during the period of PET acquisition (superior

vena cava SUV_{mean} 2.73±0.51 at 40-70 min post-injection). The optimum

contrast between 18F-fluciclatide uptake in the site of infarction compared to

the blood pool was observed at 40 min (Figure 2B). This time point was

therefore used for subsequent static imaging.

Using a 2-compartment Patlak model,[5] 18F-flucicatide uptake displayed a

distinct linear phase and a steep Ki slope, in keeping with irreversible binding

of 18F-fluciclatide to $\alpha_v\beta_3$ integrin during the 70-min period of evaluation

(Figure 2D). The three-dimensional parametric images generated from Patlak

analysis (Figure 2E, Figure 3F and Video 1) confirmed regions of increased

18F-fluciclatide binding in sites of acute infarction, supporting an up-regulation

of $\alpha_v\beta_3$ integrin within the infarct zone.

Static 18F-Fluciclatide PET in Myocardial Infarction

Using static PET images the interobserver reproducibility assessing 18F-

fluciclatide uptake in the myocardium was good (Table S2). Briefly,

quantifying focal uptake in acute infarction was most reproducible using the

TBR_{mean} method, showing no fixed or proportional biases (mean % difference

3.0 [95% CI -24.0 to 29.9]) and a high ICC value (0.94 [95% CI 0.83-0.98]).

This measure was therefore preferentially used for subsequent analysis.

Quantification of the regional 18F-fluciclatide TBR_{mean} in individual myocardial

segments also proved reproducible with no fixed or proportional biases (mean

% difference -8.97 [95% CI -31.6 to 13.6]) and a high ICC value (0.90 [95% CI

0.590-0.975], Table S3).

All patients in the acute MI cohort had increased focal myocardial uptake of 18F-fluciclatide on baseline PET/CT scanning (12±4 days after MI), which co-localized to regions of infarction on CMR (Figures 2 & 3, Tables 2 & 3, Videos 1 & 2). Hepatic uptake of 18F-fluciclatide was common. However, in the patient with inferior MI, basal inferior and infero-septal myocardial uptake of 18F-fluciclatide was quantifiable. 18F-Fluciclatide uptake was greater in the acute myocardial infarct when compared to regions of old infarction in the CTO cohort and healthy myocardium in the control group, regardless of the measure of PET uptake used (for example, TBR_{mean} 1.34±0.22 vs. 0.70±0.14 vs. 0.70±0.10, p<0.001 respectively). Indeed, no focal increase in 18F-fluciclatide uptake was observed in regions of chronic infarction, with similar PET uptake measurements compared to control subjects (e.g. TBR_{mean}, p=0.83). In regions of myocardium remote to the site of acute infarction, 18F-fluciclatide activity was modestly but uniformly increased when compared to comparative regions in CTO patients (TBR_{mean} 0.85±0.17 vs 0.64±0.12, p=0.009). Across our population there were no age-related (TBR_{mean}, r=-0.19 [-0.53-0.19], p=0.31) or sex-related (TBR_{mean} 1.14±0.07 vs. 1.25±0.17, p=0.46) differences in 18F-fluciclatide uptake.

Seventeen subjects agreed to return for a second 18F-fluciclatide PET/CT 76±19 days post-MI, with similar results noted. All these patients were clinically stable between the scans. 18F-Fluciclatide uptake remained elevated at the site of infarction (MI vs. CTO group, TBR_{mean} 1.20±0.21 vs. 0.70±0.15 respectively, p<0.001), although the intensity was reduced compared to earlier imaging (p=0.01; Figure 3). Increased 18F-fluciclatide

uptake also persisted in regions of remote myocardium when compared to uptake in CTO patients (TBR$_{mean}$ 0.82±0.15 vs 0.64±0.12 respectively, p=0.01) and interestingly remained equivalent in terms of intensity compared to the initial PET scan (TBR$_{mean}$ 0.85±0.17 vs 0.82±0.15 respectively, p=0.38).

Myocardial 18F-Fluciclatide Uptake and Cardiac Function

The extent of 18F-fluciclatide uptake following MI was compared with clinical and imaging measures of MI severity and subsequent repair (Table S3). Although segmental 18F-fluciclatide uptake displayed a moderate correlation with the degree of extracellular volume on CMR T1 mapping (r =0.37, p<0.001), it did not correlate with many of the standard measures of infarct severity, in particular there were no associations with infarct size on CMR (r=0.03, p=0.90), LVEF (r=-0.08, p=0.72), hs-TnI (r=0.13, p=0.36) or C-reactive protein (r=-0.20, p=0.38) (Table S3). This may be explained by the absence of increased uptake in the largest akinetic infarcts (normal wall motion vs. akinetic segments; TBR$_{mean}$ 0.80±0.26 vs. 0.77±0.21, p=0.77). Rather 18F-fluciclatide activity was highest in segments with hypokinesis (WMI 1&2 vs. 0; TBR$_{mean}$ 0.92±0.03 vs 0.80±0.26, p<0.001; Figure 4) and segments associated with a subendocardial pattern of LGE (subendocardial LGE vs no LGE; TBR$_{mean}$ 0.95±0.06 vs. 0.75±0.03 respectively, p<0.001; Figure 4).

18F-Fluciclatide uptake was higher in hypokinetic regions that subsequently demonstrated functional recovery compared to regions with no change or a

worsening in contractile function (TBR$_{mean}$ 0.95±0.33 vs 0.81±0.02

respectively, p=0.002; Figure 4, Video 2). Using logistic regression analysis,

18F-fluciclatide TBR$_{mean}$ emerged as a predictor of recovery in segmental

cardiac function on univariable analysis (OR 1.27 [95% CI 1.08-1.50] per 10%

increase in TBR$_{mean}$, p=0.003), which persisted after adjustment for age and

sex (OR 1.27 [95% CI 1.07-1.51] per 10% increase in TBR$_{mean}$, p=0.005). This

effect was however attenuated following additional adjustment for the

transmurality of LGE (OR 1.03 [95% CI 0.83-1.26] per 10% increase in

TBR$_{mean}$, p=0.80) and ECV (OR 1.02 [0.91-1.32] per 10% increase in

TBR$_{mean}$, p=0.35).

Discussion

Using the novel radiotracer 18F-fluciclatide, we have for the first time described the temporal expression of myocardial $\alpha_v\beta_3$ integrin receptor in patients with recent acute MI. We demonstrate intense early uptake attributable to regions of recent infarction, in particular subendocardial, hypokinetic infarcts that appeared to demonstrate subsequent functional recovery. Our data suggest that $\alpha_v\beta_3$ integrin receptor expression can be readily quantified in the infarct zone, and that 18F-fluciclatide PET may hold promise as a clinical biomarker of healing activity with application to novel pharmacological or cell-based therapies aimed at improving outcome after MI.

Expression of $\alpha_v\beta_3$ integrin by vascular endothelial cells facilitates myocardial salvage through angiogenesis in the peri-infarct zone, while also mediating the activated macrophage response to inflammatory signals and governing myofibroblast differentiation through the activation of latent TGF-β1.[9-11] The $\alpha_v\beta_3$ integrin contains a binding site for an RGD-peptide subunit (the arginine-glycine-aspartate motif) and this is the target for a number of molecular imaging probes. In murine and human studies of acute MI, RGD-based radiotracers accumulate at the site of infarction as early as 3 days, peaking at 1-3 weeks post-MI [4,12] and correlating with adverse remodeling and infarct scar formation at 12 months.[13,14] For the first time, we have here confirmed and extended these findings using the highly selective and sensitive PET RGD-radiotracer, 18F-fluciclatide. Moreover, given the study sample size and comprehensive imaging assessment, we have been able to make several

significant observations as well as incorporate a number of important controls and comparisons.

We have compared 18F-fluciclatide uptake in patients with recent acute MI with healthy control subjects and patients with established infarction. We have demonstrated that ^{18}F-fluciclatide uptake is specific for acute infarction and does not bind to old established infarcts. Perhaps more importantly, we did not see a correlation with acute infarct size, quantified as the mass of LGE on CMR. Indeed binding of 18F-fluciclatide in akinetic infarcts was relatively low, and was instead highest in sub-endocardial infarcts associated with hypokinesia. This would suggest that 18F-fluciclatide uptake is not a surrogate of infarction itself but relates more to the tissue healing response to injury.

There are a number of potential explanations for the preferential binding of 18F-fluciclatide to subendocardial infarcts. It is possible that microvascular obstruction in larger infarcts prevented tissue penetration by 18F-fluciclatide or that the presence of tissue necrosis resulted in loss of tissue architecture. However a number of our observations suggest that 18F-fluciclatide uptake reflects novel $\alpha_v\beta_3$ integrin expression due to re-endothelialisation and angiogenesis in the peri-infarct zone. First, *ex-vivo* histological examination 2 weeks following MI demonstrated that $\alpha_v\beta_3$ integrin expression predominantly co-localizes within endothelial cells of the microvasculature. Second, increased ^{18}F-fluciclatide uptake was associated with functional recovery of hypokinetic infarcts. Third, we did not observe 18F-fluciclatide uptake in

patients with CTO who have chronic and well established collateral vasculature. Fourth we did not observe large regions of microvascular obstruction on CMR imaging. This suggests that only newly forming vessels or repopulation of vessels with endothelial cells will result in $\alpha_v\beta_3$ integrin expression and ^{18}F-fluciclatide uptake. This is consistent with similar observations in other diseased states such as angiogenesis associated with malignancy.[5,7] In our patients with MI, intense binding was observed in the peri-infarct regions of sub-endocardial MIs with only poorly-defined uptake in the central necrotic area. Given these associations and the likelihood that 18F-fluciclatide identifies areas of re-endothelialisation and angiogenesis, it is perhaps not surprising that 18F-fluciclatide uptake appeared to localise to segments that demonstrated subsequent functional recovery. Taken together our data suggest that assessing $\alpha_v\beta_3$ integrin expression in the acute phase of repair might be of use in investigating the healing processes that occur following acute MI. Larger studies are required to confirm these initial findings and assess whether 18F-fluciclatide PET provides incremental benefit to CMR (our study was not sufficiently powered). However as a marker of activity 18F-fluciclatide may be of particular use in assessing the effects of novel therapies aimed at accelerating repair post-MI.

At 10 weeks following MI, 18F-fluciclatide uptake persisted in the region of infarction but was reduced compared to the 2-week assessment. This delayed phase of repair is characterized pathologically by a reduction in inflammation and angiogenesis, and a more moderated reorganization of the ECM through myofibroblast-driven type I and III collagen production.[15] From our study, we

are unable to determine whether this reduction in 18F-fluciclatide uptake

reflects the waning of re-endothelialisation and angiogenesis, or represents a

switching to myofibroblast cell types indicative of an enhanced fibrotic

response. There was some heterogeneity in the time course of 18F-

fluciclatide uptake since uptake increased at 10 weeks in 6 subjects.

However, we detected no adverse effects of this increase in uptake and there

was no corresponding increase in LGE or ECV on T1 mapping.

Modification of the extracellular matrix following MI is not only limited to the

site of infarction. Indeed, the myofibroblast-driven fibrotic expansion seen in

the remote myocardium influences global myocardial recovery.[16]

Expression of $\alpha_v\beta_3$ integrin in remote myocardial regions has been reported up

to 6 months following MI.[10,17] In keeping with this, 18F-fluciclatide activity

was consistently increased in the remote myocardium at both 2 and 10 weeks

when compared to comparative myocardial regions in patients with CTO, and

healthy controls.

There are some limitations of our study that we should acknowledge. First,

despite accounting for systolic motion using electrocardiographic gating,

cardiac PET is also limited by respiratory motion and this may affect

sensitivity in particular due to the high activity in the closely adjacent blood

pool and hepatic tissue. This is likely to be a particular problem for inferior

infarcts (present in only one of our study subjects), although these less

commonly lead to adverse remodelling and heart failure. Novel motion

tracking may in the future help to negate some of these issues and enable

even greater definition of regional $\alpha_v\beta_3$ integrin expression.[18] Second,

limited cardiac tissue was available for histological assessment, preventing

complete stoichiometric and temporal assessment of $\alpha_v\beta_3$ integrin expression

in man post-MI. Fortunately inference can be drawn from extensive animal

models of infarction, but for future application of 18F-fluciclatide a more

extensive histological assessment would be preferred. Third, our study was

not powered to address the incremental value of 18F-fluciclatide PET over

established predictors markers of cardiac recovery such as CMR. This will

require larger patient populations. Instead this study provides the first

description of increased 18F-fluciclatide in the myocardium following MI,

indicating that it provides important information about the LV remodeling

response. Further studies will be required to establish the clinical utility of this

approach.

In conclusion, we report the largest and most comprehensive analysis of an

$\alpha_v\beta_3$ integrin radiotracer in the assessment of myocardial repair following

acute MI. We have demonstrated that increased 18F-fluciclatide uptake

occurs at sites of acute myocardial infarction, in particular regions of sub-

endocardial infarction and hypokinesia associated with subsequent functional

recovery. Our data suggest myocardial $\alpha_v\beta_3$ integrin expression represents a

marker of ongoing cardiac repair, and that 18F-fluciclatide is a potentially

useful imaging biomarker for investigating this healing response post-MI.

Disclosures

None.

24

123456789 10 11 12 13 14 15 16 17 18 19 20 21 22 23 24 25 26 27 28 29 30 31 32 33 34 35 36 37 38 39 40 41 42 43 44 45 46 47 48 49 50 51 52 53 54 55 56 57 58 59 60

References

1   Lewis EF, Moye LA, Rouleau JL, *et al.* Predictors of late development of heart failure in stable survivors of myocardial infarction: the CARE study. *J Am Coll Cardiol* 2003;**42**:1446–53.

2   Sutton MGSJ, Sharpe N. Left Ventricular Remodeling After Myocardial Infarction. *Circulation* 2000;**101**:2981-2988

3   Meoli DF, Sadeghi MM, Krassilnikova S, *et al.* Noninvasive imaging of myocardial angiogenesis following experimental myocardial infarction. *J Clin Invest* 2004;**113**:1684–91. doi:10.1172/JCI200420352

4   Higuchi T, Bengel FM, Seidl S, *et al.* Assessment of v 3 integrin expression after myocardial infarction by positron emission tomography. *Cardiovascular Research* 2008;**78**:395–403. doi:10.1093/cvr/cvn033

5   Kenny LM, Coombes RC, Oulie I, *et al.* Phase I trial of the positron-emitting Arg-Gly-Asp (RGD) peptide radioligand 18F-AH111585 in breast cancer patients. *Journal of Nuclear Medicine* 2008;**49**:879–86. doi:10.2967/jnumed.107.049452

6   McParland BJ, Miller MP, Spinks TJ, *et al.* The biodistribution and radiation dosimetry of the Arg-Gly-Asp peptide 18F-AH111585 in healthy volunteers. *Journal of Nuclear Medicine* 2008;**49**:1664–7. doi:10.2967/jnumed.108.052126

7   Tomasi G, Kenny L, Mauri F, *et al.* Quantification of receptor-ligand binding with [18F]fluciclatide in metastatic breast cancer patients. *Eur J Nucl Med Mol Imaging* 2011;**38**:2186–97. doi:10.1007/s00259-011-1907-9

8   Cerqueira MD, Weissman NJ, Dilsizian V, *et al.* Standardized myocardial segmentation and nomenclature for tomographic imaging of the heart. A statement for healthcare professionals from the Cardiac Imaging Committee of the Council on Clinical Cardiology of the American Heart Association. *Circulation* 2002. 539–42.

9   Sarrazy V, Koehler A, Chow ML, *et al.* Integrins αvβ5 and αvβ3 promote latent TGF-β1 activation by human cardiac fibroblast contraction. *Cardiovascular Research* 2014;**102**:407–17. doi:10.1093/cvr/cvu053

10   Sun M. Temporal Response and Localization of Integrins beta1 and beta3 in the Heart After Myocardial Infarction: Regulation by Cytokines. *Circulation* 2003;**107**:1046–52. doi:10.1161/01.CIR.0000051363.86009.3C

11   Antonov AS, Antonova GN, Munn DH, *et al.* αVβ3 integrin regulates macrophage inflammatory responses via PI3 kinase/Akt-dependent NF-κB activation. *J Cell Physiol* 2011;**226**:469–76. doi:10.1002/jcp.22356

12 Sun Y, Zeng Y, Zhu Y, *et al.* Application of (68)Ga-PRGD2 PET/CT for
    αvβ3-integrin imaging of myocardial infarction and stroke. *Theranostics*
    2014;**4**:778–86. doi:10.7150/thno.8809

13 Sherif HM, Saraste A, Nekolla SG, *et al.* Molecular imaging of early αvβ3
    integrin expression predicts long-term left-ventricle remodeling after
    myocardial infarction in rats. *J Nucl Med* 2012;**53**:318–23.
    doi:10.2967/jnumed.111.091652

14 Verjans J, Wolters S, Laufer W, *et al.* Early molecular imaging of
    interstitial changes in patients after myocardial infarction: Comparison
    with delayed contrast-enhanced magnetic resonance imaging. *Journal of
    Nuclear Cardiology* 2010;**17**:1065–72. doi:10.1007/s12350-010-9268-5

15 Plein S, Kidambi A. Understanding LV Remodeling Following Myocardial
    Infarction. *J Am Coll Cardiol* 2012;**5**:894–6.
    doi:10.1016/j.jcmg.2012.07.006

16 Carrick D, Haig C, Rauhalammi S, *et al.* Pathophysiology of LV
    Remodeling in Survivors of STEMI: Inflammation, Remote Myocardium,
    and Prognosis. *JACC Cardiovasc Imaging* 2015;**8**:779–89.
    doi:10.1016/j.jcmg.2015.03.007

17 van den Borne SWM, Diez J, Blankesteijn WM, *et al.* Myocardial
    remodeling after infarction: the role of myofibroblasts. *Nat Rev Cardiol*
    2009;**7**:30–7. doi:10.1038/nrcardio.2009.199

18 Rubeaux M, Joshi N, Dweck MR, *et al.* Motion correction of 18F-sodium
    fluoride PET for imaging coronary atherosclerotic plaques. *J Nucl Med*
    2015;:jnumed.115.162990. doi:10.2967/jnumed.115.162990

Figure Legends

Figure 1. α$_v$β$_3$ Integrin Expression in Patient with Recent Myocardial Infarction

Adjacent fresh frozen and cryosectioned biopsies from the peri-infarct area of a patient with recent anterior MI. Immunohistochemical staining for **(A)** α$_v$β$_3$ integrin displayed multiple regions of positive staining that co-localize to regions of staining for vascular endothelial cells (CD31, **B**) visible at x4 magnification. At x20 magnification, these regions of α$_v$β$_3$ staining **(C)** correspond predominantly to arterioles and the microvasculature **(D)**, and also to regions of staining for smooth muscle actin **(E)**, representative of both arterioles (co-staining with CD31) and myofibroblasts. There were relatively few macrophages **(F)**.

Figure 2. Dynamic Analysis of 18F-Fluciclatide Uptake

Axial and sagittal CT angiography of the thorax in a patient with recent anterior MI **(A).** The time-activity curves generated from the descending aorta and the apical interventricular septum (blue crosshairs) show increased uptake in the infarct relative to blood pool. Optimal contrast between 18F-fluciclatide tissue and blood pool activity was observed after 40 min (dotted line, **B**). The PET image in the axial and sagittal plane shows increased uptake within the apical septum, although there is some background activity **(C).** Patlak analysis of ROI's placed in the interventricular septum confirms integrin binding, as evidenced by the gradient of the slope and the y-intercept **(D),** and using a Ki-generated image we can better identify and delineate focal uptake within myocardium **(E)**. A region of remote myocardium within the

same patient generates a Patlak curve with significantly lower gradient and intercept in comparison **(F)**.

Figure 3. 18F-Fluciclatide Uptake in Acute Myocardial Infarction

18F-Fluciclatide uptake in 3 patients with recent subendocardial myocardial infarction (MI). Patient 1, 13 days after anterior MI, displaying a short-axis PET image of the left ventricle with crescentric 18F-fluciclatide uptake **(A)** that correlates with the interventricular septum and anterior wall on CT angiography **(B)**. The fused PET/CT-angiography image **(C)** shows this uptake corresponds exactly to the region of late gadolinium enhancement (LGE) on CMR **(D)**. Further delineation of myocardial uptake on PET/CT is clearer in the 2-chamber view **(E)** and on a fused CT/3D-Patlak image, which shows this uptake to follow a watershed-pattern emerging from the coronary stents present in the left anterior descending coronary artery **(F)** (see Video File 1). Panels **G & H:** patient 2, 8 days following anterior MI, displaying focal uptake of 18F-fluciclatide in the anterior wall and apex in the 3-chamber view on PET/CT **(G)** which corresponds to the region of infarction on LGE CMR imaging **(H).** Panels **I & J**: patient 3, showing focal uptake of 18F-fluciclatide in the inferior wall 19 days following MI on PET/CT **(I)** that again corresponds to the infarction on CMR LGE imaging **(J)**.

Figure 4. 18F-Fluciclatide Uptake in Myocardial Infarction

Uptake of 18F-fluciclatide in **(A)** patients with acute myocardial infarction at 2 and 10 weeks, patients with chronic total occlusion and healthy control subjects. Uptake was greatest at 2 weeks after myocardial infarction **(B).** 18F-Fluciclatide uptake in the acute MI group was greater in regions of

hypokinesis when compared to sites of normal function or akinesis (**C**). This

translated to a higher 18F-fluciclatide uptake in those regions which

subsequently improved in function on follow-up CMR (**D**).

Tables

Table 1. Baseline Participant Characteristics

	All	Acute Myocardial Infarction Group	Chronic Total Occlusion Group	Control Group	*p* value*
	(n=37)	(n=21)	(n=7)	(n=9)	
Patient Characteristics					
Age (years)	64±10	62±12	69±7	66±7	*0.06*
Male Sex	27(73)	16(76)	5(71)	6(67)	*0.46*
BMI (kg/m^2)	28±4	28±5	31±3	27±4	*0.74*
18F-Fluciclatide Dose (mBq)	229±12	227±13	227±14	232±9	*0.86*
Current Smoker	9(24)	8(38)	1(14)	0(0)	*0.01*
Diabetes Mellitus	4(11)	3(14)	1(14)	0(0)	*0.06*
Hypertension	16(43)	7(33)	5(71)	4(44)	*0.04*
Hypercholesterolemia	22(60)	14(66)	6(86)	2(22)	*<0.001*
Cardiovascular History					
Prior myocardial infarction	7(19)	1(5)	6(86)	0(0)	*<0.001*
Angiographically documented CAD	28(76)	21(100)	7(100)	0(0)	*<0.001*
Previous PCI	4(11)	1(5)	3(42)	0(0)	*<0.001*
CCS Class					
0	28(76)	17(81)	2(29)	9(100)	*0.02*
I or II	7(19)	4(19)	3(42)	0(0)	*0.03*
III or IV	2(6)	0(0)	2(29)	0(0)	*0.51*
NYHA Class					
I	29(78)	15(71)	3(42)	9(100)	*0.32*
II	7(19)	5(24)	2(29)	0(0)	*0.39*
III or IV	2(6)	1(5)	1(14)	0(0)	*0.25*
Medications					
Aspirin	27(73)	21(100)	6 (86)	0(0)	*<0.001*
Clopidogrel	22(59)	19(90)	3(42)	0(0)	*<0.001*
Statin	29(78)	21(100)	7(100)	1(11)	*0.004*
β-Blocker	26(70)	20(95)	6(86)	0(0)	*<0.001*
ACEi / ARB	27(73)	20(95)	5(71)	2(22)	*0.02*
Clinical Features					
Systolic BP (mm Hg)	137±22	128±18	140±24	155±21	*0.06*
Heart rate (bpm)	64±12	62±13	61±11	68±10	*0.42*
Creatinine (µmol/L)	79±15	82±19	77±14	73±12	*0.54*
hs-CRP (mg/L)	3.5[1.3-9.8]	5.6[2.0-11.7]	2.2[1.0-9.1]	1.5[1.2-3.3]	*0.008*

Mean±SD, median [IQR] or number (percentage). *Analysis of variance, Students t-test (continuous data) or Chi squared test (categorical data).

Abbreviations: BMI, body-mass index; CAD, coronary artery disease; PCI, percutaneous coronary intervention; CCS, Canadian Cardiovascular Society; NYHA, New York Heart Association; ACEi, angiotensin-converting enzyme inhibitor, ARB, angiotensin receptor blocker; BP, blood pressure; hs-CRP, high-sensitivity c-reactive protein

Table 2. Baseline Imaging Assessment

	All	Acute Myocardial Infarction Group	Chronic Total Occlusion Group	Control Group	*p value**
	(n=37)	(n=21)	(n=7)	(n=9)	
CMR Imaging					
LVEF (%)	58±10	52±9	62±8	65±5	*<0.001*
LV Mass (indexed,g/m^2)	79±20	85±20	66±17	75±16	*0.07*
LVEDV (mL/m^2)	77±18	80±18	69±13	76±17	*0.35*
LVESV (mL/m^2)	34±13	39±14	30±10	27±9	*0.046*
WMI	0.25±0.13	0.40±0.20	0.09±0.05	0.0±0.0	*<0.001*
ECV (%)	31±5	34±4	28±3	28±2	*<0.001*
Presence of LGE	27(73)	21(100)	6(86)	0(0)	*<0.001*
Infarct size (g/m^2)	8±8	12±7	8±8	0±0	*<0.001*
PET Imaging					
SUV_{mean} (kBq/mL)					
SVC	2.73±0.51	2.85±0.51	2.57±0.39	2.58±0.57	*0.27*
Total LV uptake	2.24±0.51	2.33±0.48	1.96±0.53	1.77±0.27	*<0.001*
Myocardial Infarct Uptake	3.23±1.03	3.72±0.63	1.76±0.26	-	*<0.001*
Remote Myocardial Uptake	2.21±0.60	2.41±0.57	1.62±0.14	-	*0.001*
TBR_{mean}					
Total LV Uptake	0.77±0.16	0.82±0.18	0.71±0.06	0.70±0.03	*0.08*
Myocardial Infarct Uptake	1.05±0.37	1.34±0.22	0.70±0.14	-	*<0.001*
Remote Myocardial Uptake	0.80±0.18	0.85±0.17	0.64±0.12	-	*0.009*
SUV_{max} (kBq/mL)					
Total LV uptake	2.71±0.58	2.86±0.56	2.24±0.40	2.07±0.31	*<0.001*
Myocardial Infarct Uptake	3.53±1.00	3.98±0.68	2.18±0.35	-	*<0.001*
Remote Myocardial Uptake	2.59±0.64	2.75±0.65	2.18±0.35	-	*0.02*
TBR_{max}					
Total LV uptake	0.98±0.19	1.02±0.19	0.89±0.20	0.81±0.09	*0.01*
Myocardial Infarct Uptake	1.28±0.34	1.42±0.25	0.86±0.16	-	*<0.001*
Remote Myocardial Uptake	0.94±0.19	0.97±0.20	0.84±0.13	-	*0.11*
SUV_C (kBq/mL)					
Total LV uptake	-0.55±0.57	-0.52±0.55	-0.61±0.67	0.81±0.42	*0.85*
Myocardial Infarct Uptake	0.75±0.91	1.13±0.67	-0.40±0.46	-	*<0.001*
Remote Myocardial Uptake	-0.19±0.52	-0.11±0.54	-0.45±0.37	-	*0.12*

Mean±SD or number (percentage). *Analysis of variance, Students t-test (continuous data) or Chi squared test (categorical data).

Abbreviations: CMR,cardiac magnetic resonance; LVEF,left ventricular ejection fraction; LVEDV,left ventricular end diastolic volume; LVESV,left ventricular end systolic volume; WMI,wall motion index; ECV,extracellular volume; LGE,late gadolinium enhancement; SVC; superior vena cava; SUV,standardized uptake value; TBR,tissue-to-background ratio, SUV_C, corrected SUV

Table 3.

Acute myocardial infarction assessments

CMR Imaging	Imaging Data		*p-value*
	Initial CMR	**Follow-up CMR**	
	(n=21)	**(n=17)**	
MI to CMR (days)	13±5	287±37	*<0.01*
LVEF (%)	52±9	55±8	*<0.01*
Indexed LV Mass (g/m^2)	85±20	74±13	*<0.01*
LVEDV (mL/m^2)	80±18	82±16	*0.88*
LVESV (mL/m^2)	39±14	38±12	*0.36*
Wall Motion Index	0.40±0.20	0.22±0.15	*<0.01*
ECV (%)	34±4	33±2	*0.58*
Infarct size (g/m^2)	13 [7-17]	6 [3-14]	*0.03*

PET Imaging			
	Initial PET/CT	**Repeat PET/CT**	
	(n=21)	**(n=17)**	
MI to PET (days)	12±4	76±19	<0.01
Total LV Uptake (TBR$_{mean}$)	0.82±0.18	0.85±0.18	*0.96*
Myocardial Infarct Uptake (TBR$_{mean}$)	1.34±0.22	1.20±0.21	*0.02*
Remote Myocardial Uptake (TBR$_{mean}$)	0.85±0.17	0.82±0.15	*0.38*
Segmental uptake (TBR$_{mean}$) & Regional Wall Motion (WMI)			
Normal function (0)	0.80±0.26	0.83±0.23	*0.14*
Mild-mod hypokinesia (1)	0.89±0.33	0.97±0.29	*0.33*
Severe hypokinesia (2)	0.97±0.28	0.91±0.34	*0.47*
Akinesia (3)	0.77±0.21	0.73±0.24	*0.66*
Dyskinesia (4)	-	-	-
Segmental uptake & Transmurality of MI (TBR$_{mean}$)			
No infarct	0.75±0.23	0.81±0.23	*NA*
Subendocardial infarct (1-75%)	0.95±0.29	1.08±0.28	*NA*
Transmural infarct (76-100%)	0.89±0.29	0.88±0.27	*NA*

Mean±SD or median [IQR].

Abbreviations: MI, myocardial infarction; LV, left ventricle; TBR$_{mean}$, mean tissue-to-background ratio; CMR, magnetic resonance imaging; LVEF, left-ventricular ejection fraction; LVEDV, left-ventricular end diastolic volume; LVESV, left ventricular end systolic volume; WMI, wall motion index; ECV, mean extracellular volume.
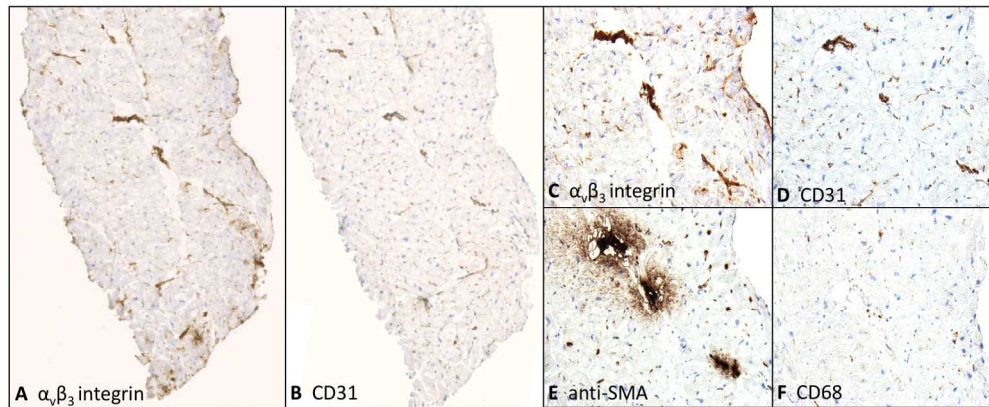
Figure 1. αvβ3 Integrin Expression in Patient with Recent Myocardial Infarction. Adjacent fresh frozen and cryosectioned biopsies from the peri-infarct area of a patient with recent anterior MI. Immunohistochemical staining for (A) αvβ3 integrin displayed multiple regions of positive staining that co-localize to regions of staining for vascular endothelial cells (CD31, B) visible at x4 magnification. At x20 magnification, these regions of αvβ3 staining (C) correspond predominantly to arterioles and the microvasculature (D), and also to regions of staining for smooth muscle actin (E), representative of both arterioles (co-staining with CD31) and myofibroblasts. There were relatively few macrophages (F).
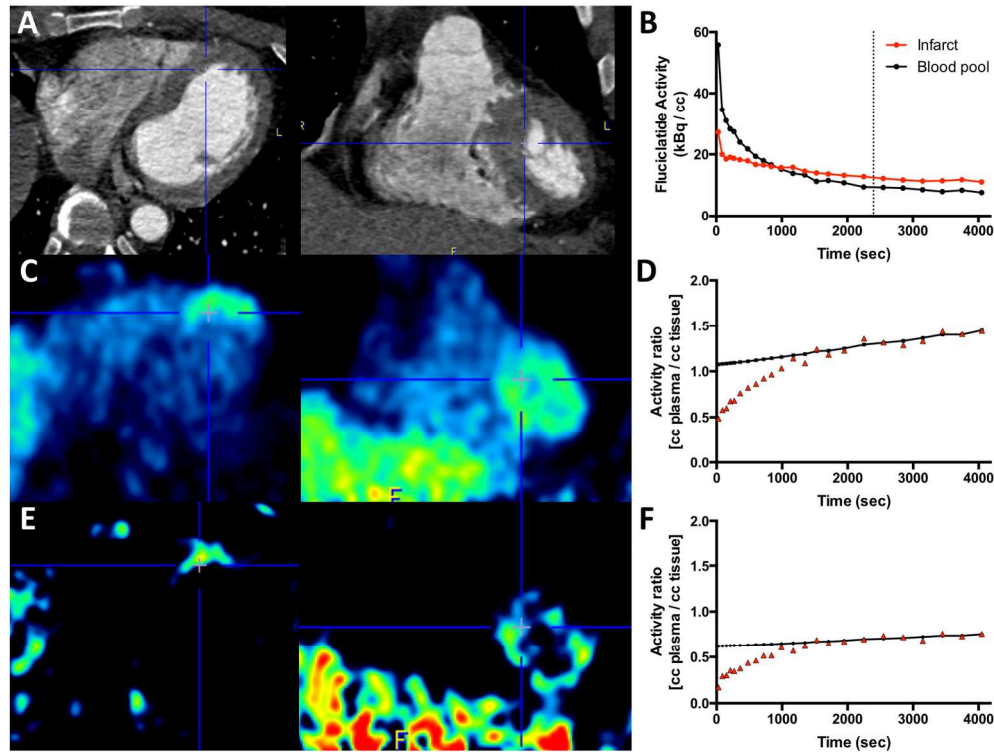
198x82mm (300 x 300 DPI)

Figure 2. Dynamic Analysis of 18F-Fluciclatide Uptake. Axial and sagittal CT angiography of the thorax in a patient with recent anterior MI (A). The time-activity curves generated from the descending aorta and the apical interventricular septum (blue crosshairs) show increased uptake in the infarct relative to blood pool. Optimal contrast between 18F-fluciclatide tissue and blood pool activity was observed after 40 min (dotted line, B). The PET image in the axial and sagittal plane shows increased uptake within the apical septum, although there is some background activity (C). Patlak analysis of ROI's placed in the interventricular septum confirms integrin binding, as evidenced by the gradient of the slope and the y-intercept (D), and using a Ki-generated image we can better identify and delineate focal uptake within myocardium (E). A region of remote myocardium within the same patient generates a Patlak curve with significantly lower gradient and intercept in comparison (F).
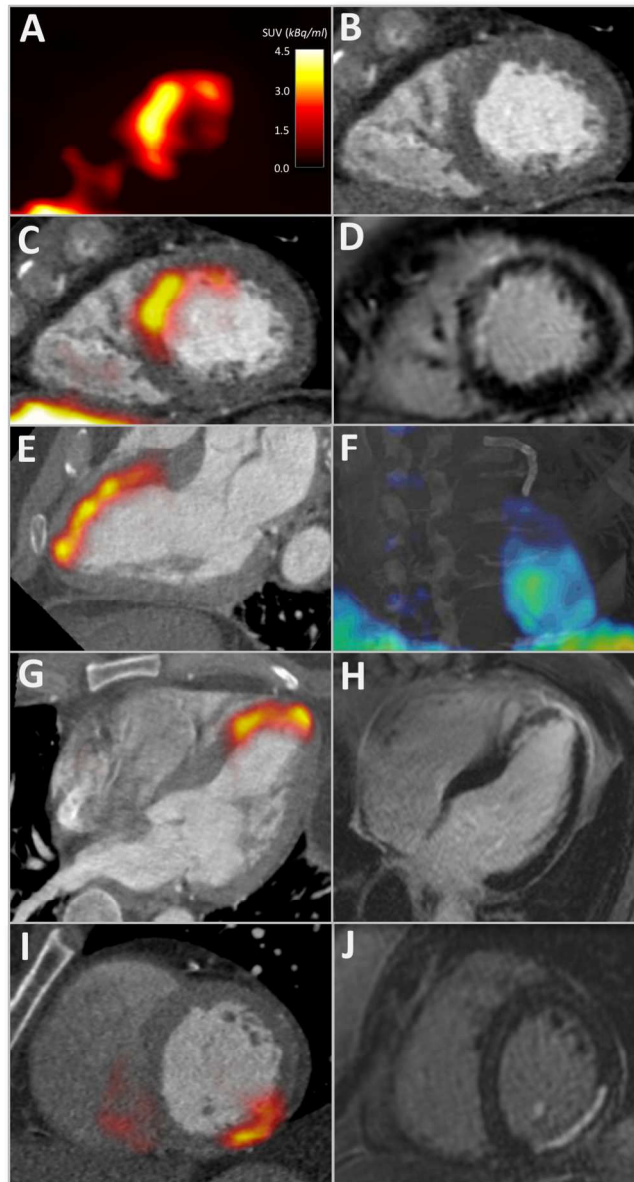
182x137mm (300 x 300 DPI)

Figure 3. 18F-Fluciclatide Uptake in Acute Myocardial Infarction. 18F-Fluciclatide uptake in 3 patients with recent subendocardial myocardial infarction (MI). Patient 1, 13 days after anterior MI, displaying a short-axis PET image of the left ventricle with crescentric 18F-fluciclatide uptake (A) that correlates with the interventricular septum and anterior wall on CT angiography (B). The fused PET/CT-angiography image (C) shows this uptake corresponds exactly to the region of late gadolinium enhancement (LGE) on CMR (D). Further delineation of myocardial uptake on PET/CT is clearer in the 2-chamber view (E) and on a fused CT/3D-Patlak image, which shows this uptake to follow a watershed-pattern emerging from the coronary stents present in the left anterior descending coronary artery (F) (see Video File 1). Panels G & H: patient 2, 8 days following anterior MI, displaying focal uptake of 18F-fluciclatide in the anterior wall and apex in the 3-chamber view on PET/CT (G) which corresponds to the region of infarction on LGE CMR imaging (H). Panels I & J: patient 3, showing focal uptake of 18F-fluciclatide in the inferior wall 19 days following MI on PET/CT (I) that again corresponds to the infarction on CMR LGE imaging (J).

1
2
3
4
5
6
7
8
9
10
11
12
13
14
15
16
17
18
19
20
21
22
23
24
25
26
27
28
29
30
31
32
33
34
35
36
37
38
39
40
41
42
43
44
45
46
47
48
49
50
51
52
53
54
55
56
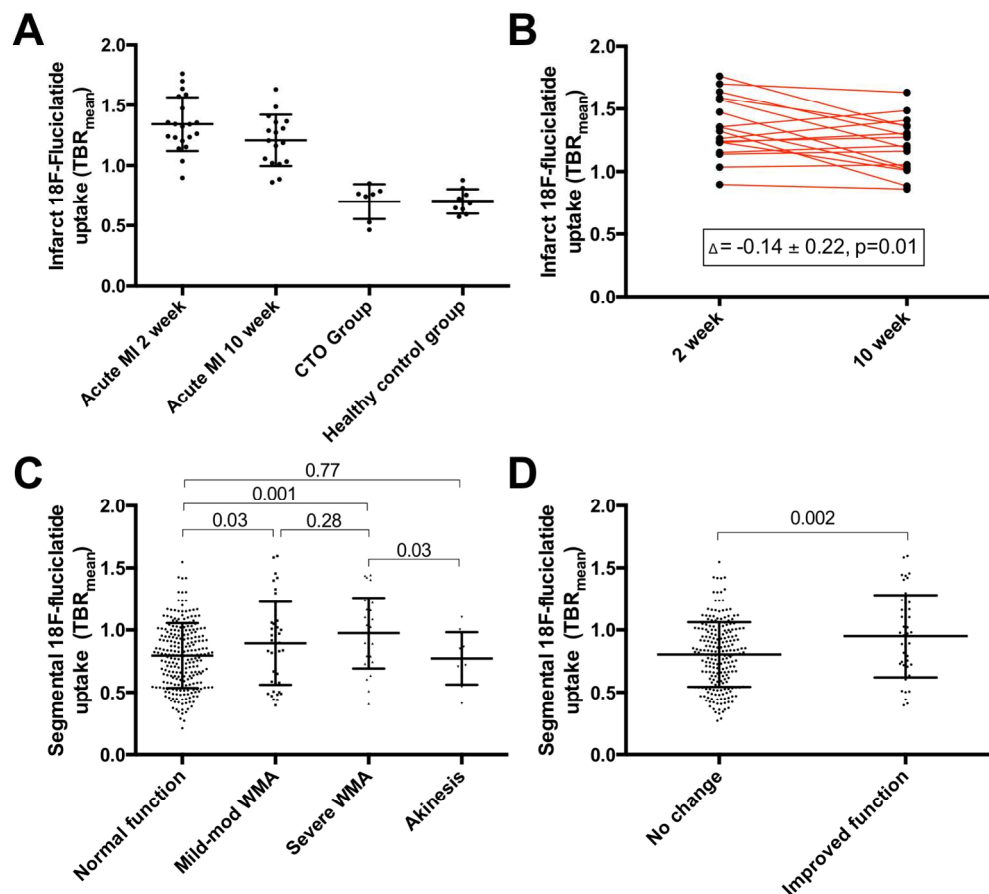57
58
59
60

97x177mm (300 x 300 DPI)

Figure 4. 18F-Fluciclatide Uptake in Myocardial Infarction. Uptake of 18F-fluciclatide in (A) patients with acute myocardial infarction at 2 and 10 weeks, patients with chronic total occlusion and healthy control subjects. Uptake was greatest at 2 weeks after myocardial infarction (B). 18F-Fluciclatide uptake in the acute MI group was greater in regions of hypokinesis when compared to sites of normal function or akinesis (C). This translated to a higher 18F-fluciclatide uptake in those regions which subsequently improved in function on follow-up CMR (D).

161x144mm (300 x 300 DPI)

Supplementary Material

Imaging Assessments

Positron Emission Tomography / Computer Tomography Imaging

All patients underwent PET-CT imaging of the thorax with a hybrid scanner (Biograph mCT, Siemens Medical Systems, Erlangen, Germany) at the Clinical Research Imaging Centre, University of Edinburgh. Subjects were administered a target dose of 230 MBq 18F-fluciclatide. An attenuation-correction CT scan (non-enhanced 120 kV and 50 mA, 3-mm slices) was performed, followed by the PET acquisition with electrocardiographic (ECG) gating. To assess tracer pharmacodynamics and the optimum timing of scanning, dynamic PET imaging of the thorax was initially performed in 10 subjects in 3-dimensional mode with a single bed position for 70 min. The remainder of study subjects underwent static imaging performed at the optimal time point (40 min post-injection) using a single 30-min bed position in list mode. To enable an accurate definition of cardiac anatomy cardiac CT angiography was performed on the hybrid scanner immediately after the PET acquisition: 330 ms rotation time, 100 (body mass index <25 kg/m^2) or 120 (body mass index >25 kg/m^2) kV tube voltage, 160-245 mAs tube current, 3.8 mm/rotation table feed, prospective (heart rate regular and <60 /min), or retrospective (heart rate >60 /min) electrocardiogram-gated. Depending on the body mass index, a bolus of 80-100 mL contrast (400 mgI/mL; Iomeron, Bracco, Milan, Italy) was injected intravenously at 5 mL/s, after determining the appropriate trigger delay with a test bolus of 20 mL contrast material.

PET Kinetic Analysis

Kinetic analysis was undertaken to investigate the uptake of 18F-fluciclatide within the myocardium. The dynamic PET data were reconstructed (Ultra-HD, 2 iterations, 21 subsets, 256 pixels, 1.6-mm pixel size) using a dynamic protocol without ECG gating in following time frames; 60s x 5, 120s x 5, 180s x 5, 300s x 8. Regions of interest (ROI's) were drawn in the descending aorta blood pool and myocardium, and used to derive time activity curves after decay correction. An input function calculation based on the PET image–derived activity curve from the aorta blood pool [1] and the myocardial time-activity curve were used to estimate the tissue influx rate Ki (the slope of the linear regression) and the volume of distribution (the y-axis intercept) using a 2-tissue irreversible Patlak model [2,3]. Thoracic 18F-fluciclatide dynamic activity was then normalized for the blood-pool input function on a voxel-by-voxel basis, and after 3D Gaussian filtering (5-mm FWHM) a parametric 3-dimensional image of 18F-fluciclatide uptake was generated (PMod version 3.409, Pmod technologies limited, Switzerland). Using this image, regions of 18F-fluciclatide binding in the myocardium were identified and manually delineated for subsequent Ki analysis.

Static Image Reconstruction and Analysis

For all patients, static ECG-gated PET images were reconstructed in diastole (40-70 min post-injection, 50–75% of the R-R interval, Ultra-HD, 2 iterations, 24 subsets, zoom x2, 200 pixels). Images were analysed by an experienced observer (WJ) using an OsiriX workstation (OsiriX version 6.0 64-bit; OsiriX Imaging Software, Geneva,

Switzerland). PET images were fused and aligned with CT angiography datasets in

diastole. Myocardial radiotracer uptake was quantified using two methods. First, using a

standardized approach PET/CT datasets were re-orientated into traditional short-axis,

2-chamber, 3-chamber and 4-chamber views with a slice thickness of 3 mm in order to

fully visualize myocardial radiotracer uptake and allow comparison with CMR imaging.

Regions of interest (ROIs) were drawn at sites that corresponded to the areas of acute

infarction seen on CMR late gadolinium enhancement imaging. To define referent

'remote' myocardial regions, ROI's were drawn within proximal regions of the

myocardial territory that displayed no CMR evidence of infarction. Care was taken to

avoid blood-pool contamination. ROIs were copied onto the PET dataset and mean

radiotracer activity measured using standard uptake values (SUV; the decay corrected

tissue concentration of the tracer divided by the injected dose per body weight) and

corrected for radiotracer blood-pool activity in the superior vena cava (SVC) to provide a

mean tissue-to-background ratio (TBR_{mean}).[4,5] Second, the CT angiography dataset

was re-orientated into the left ventricular short axis (slice thickness 8 mm). Basal, mid-

cavity, and apical regions were manually delineated into segmental ROI's according to

the standard 17-segment model recommended by the American College of

Cardiology/American Heart Association.[6] We excluded the true apex as it was not

possible to avoid partial volume effects. ROI's were then copied onto the re-orientated

PET image dataset and segmental SUV and TBR data extracted using the technique

above. In a substudy of 10 randomly selected subjects, interobserver reproducibility was

assessed by two experienced observers (WJ,CM).

MRI Imaging

Cardiac MRI was performed at 3 T (MAGNETOM Verio, Siemens AG, Healthcare

Sector, Erlangen, Germany). For the assessment of left ventricular function, short-axis

cine images from the mitral valve annulus to the apex were obtained using a balanced

steady-state free-precession sequence (8-mm parallel slices with 2-mm spacing).

Quantification of left ventricular function and volumes indexed to body surface area was

assessed with dedicated software (Siemens AG Healthcare Sector, Erlangen,

Germany). Regional systolic function assessments were performed from the basal, mid,

and apical short-axis slices by calculating the end-diastolic and end-systolic wall

thicknesses and expressed as the wall motion score index (WMSI; 0, normal; 1, mild or

moderate hypokinesia; 2, severe hypokinesia; 3, akinesia; 4, dyskinesia).[7] The

assessment of focal replacement myocardial fibrosis was performed with late

gadolinium enhancement (LGE) imaging, 15 min after administration of 0.1 mmol/kg

gadobutrol (Gadovist/Gadavist, Bayer Pharma AG, Berlin, Germany). An inversion

recovery fast gradient-echo sequence was applied to the left ventricular short-axis stack

with the inversion time optimized to achieve satisfactory nulling of the myocardium. The

amount of LGE was quantified with QMASS software (Medis Medical Imaging Systems,

Leiden, the Netherlands) using a signal intensity threshold greater than twice the

standard deviation above the mean value in a normal region of myocardium sampled on

the same short-axis image. The transmural extent of infarction within each segment was

classified using a transmurality score (transmurality index; 0, no LGE; 1, 1-50%; 2, 51-

75% or 3, 76-100%) and recorded as either subendocardial (1-2) or transmural (3).[8]

Areas thought to represent inversion artefact or blood pool contamination were manually excluded. Myocardial extracellular volume fraction (ECV) has been demonstrated to act as a measure of myocardial fibrosis in a variety of cardiac conditions.[9,10] Recently, our group has described a highly reproducible standardized approach to analyze myocardial ECV. [11] Briefly, myocardial T1 mapping was performed in the mechanism cohort using the modified look-locker inversion recovery sequence: flip angle, 35°; minimum TI, 100 ms; TI increment, 80 ms; and time delay, 150 ms with a heartbeat acquisition scheme of 3-3-5. [12] Regions of interest were drawn around the myocardium on the short-axis, pre-contrast, motion-corrected myocardial T1 maps and copied onto corresponding 20-min post-contrast maps, with minor adjustments made to avoid partial volume effects and artifact (OsiriX version 4.1.1, Geneva, Switzerland). ECV was calculated according to the following formula:

$$ECV = (\Delta R1_{myocardium}/\Delta R1_{blood\text{-}pool}) \times (1 - hematocrit)$$

where:

$$\Delta R1 = (1/postcontrast\ T1 - 1/precontrast\ T1).$$

Hematocrit was sampled at the time of MRI. [13]

Histological Assessment

For histological analysis, myocardial biopsy samples were obtained from patients undergoing coronary artery bypass grafting following myocardial infarction. Patients with recent large ST-elevation myocardial infarction (<14 days, hs-cTnI >10,000 ng/L) were considered for inclusion. A core cardiac biopsy was taken intra-operatively under direct

visualisation by an experienced surgeon from the peri-infarct zone. Samples were fresh frozen and mounted in cryosection medium. The tissue samples were then cut in sequential, longitudinal 4-μm sections at -20 °C and thaw-mounted onto microscope slides. They were dried for 15 min and spray-fixed with neutral buffered formalin. After rinsing in distilled water, sections were stained with hematoxylin-eosin (HE) and van-Gieson (VG) for conventional histopathological examination. In order to optimize immunohistochemistry, an antigen-unmasking step was performed by microwave treatment for 30 s. Endogenous peroxidase was blocked by incubation with hydrogen peroxide for 5 min. Sections were subsequently incubated with the primary antibodies; smooth muscle actin, CD31, CD68 (clone PG-M1), and integrin $\alpha_v\beta_3$ antibody, clone LM609 (Millipore) for 30 min at room temperature. After washing the sections were incubated with Envision Flex (DAKO, K5007) for 30 min at room temperature, followed by incubation with diaminobenzamine (Sigma) for 10 min. The slides were finally counterstained with hematoxylin and digitally imaged (Axioscan.Z1, Zeiss, UK) before assessment.

PET Repeatability Studies

The reproducibility of 18F-fluciclatide uptake quantification was assessed in both the blood pool and the myocardium in 10 subjects selected at random. Residual blood pool radiotracer activity was quantified within both the SVC and right atrium. While both methods displayed no fixed or proportional biases with narrow limits of agreement and high ICC values of >0.94, the SVC-approach appeared to hold a slight advantage (ICC 0.97 [95% CI; 0.93-0.99]) and this therefore was applied throughout the study to quantify latent radiotracer blood activity (supplementary table 1). Quantification of

radiotracer uptake within the region of myocardial infarction was assessed using the mean Standard Uptake Value (SUV_{mean}), the mean tissue to background ratio (TBR_{mean}) and a novel method subtracting the target tissue mean SUV from the blood pool mean SUV ($SUV_{target – blood pool}$).[14] The SUV_{mean} and TBR_{mean} both proved highly reproducible, displaying no fixed or proportional biases (mean % difference [95% limits of agreement]; 3.0 [-27.2 - 33.3], and 3.0 [-24.0-29.9] respectively) and a high ICC value (0.93 [0.82-0.97] and 0.940 [0.83-0.98] respectively). Selecting repeatable regions of remote myocardium proved less reliable, with wider limits of agreement (-18.9-66.2) and a moderate intra-class coefficient value of 0.60. The TBR_{mean} method was selected for the study to compensate for potential contamination from residual blood pool activity.

To quantify segmental myocardial uptake, a 16-segment model approach using both the TBR_{mean} the SUV_{mean} quantification methods appeared reliable, again with no fixed or proportional bias and reasonable limits of agreement (mean % difference, -8.97 [-31.6-13.6] and -6.7 [-25.3-11.9], respectively) and an excellent ICC of 0.90 and 0.96 respectively (Table 1). The TBR_{mean} approach was selected for the study again to compensate for potential blood pool contamination,

Supplementary Table 1. Characteristics of patients with acute myocardial infarction

Clinical Data	Acute MI Group (n=21)
Peak cardiac troponin I (ng/L)	50,000 [26,753-50,000]
Percutaneous coronary intervention	20 (95)
Symptom onset to reperfusion (min)	197 [148-342]
Single vessel disease	10 (48)
Myocardial Infarction Territory	
Anterior	16 (76)
Lateral	4 (19)
Inferior	1 (5)
Adverse Outcome	
TIMI Flow post-PCI <3	1 (5)
Cardiogenic Shock	3 (14)
IABP	2 (10)
Aborted cardiac arrest	2 (10)

Median [interquartile range] and number (%).

Abbreviations; TIMI, trials in myocardial infarction; PCI, percutaneous coronary intervention;

IABO, intra-aortic balloon pulsation

Supplementary Table 2. 18F-Fluciclatide Reproducibility

	Reproducibility Analysis	
	Mean % difference[a]	Intra-class coefficient[b]
Blood pool assessment (SUV)		
SVC	3.1 (-9.5–15.6)	0.971 (0.928-0.989)
Right Atrium	-0.46 (-11.7-10.7)	0.943 (0.868-0.975)
Infarct assessment		
TBR_{mean}		
Whole Ventricle	-8.97 (-31.6-13.6)	0.898 (0.590-0.975)
Infarct	3.0 (-24.0-29.9)	0.940 (0.833-0.978)
Remote myocardium	23.7 (-18.9-66.2)	0.604 (-0.280-0.847)
SUV_{mean}		
Whole ventricle technique	-6.7 (-25.3–11.9)	0.957 (0.830-0.989)
Infarct	3.0 (-27.2-33.3)	0.930 (0.819-0.973)
Remote myocardium	21.2 (-11.1-53.7)	0.787 (0.448-0.918)
Infarct:remote myocardium ratio	-18.2 (-60.6-24.1)	0.687 (0.187-0.879)
SUV_{target tissue - blood pool}		
Whole Ventricle	24.1 (-19.2–67.3)	0.410 (-0.372-0.698)
Infarct	77.7 (-464.6–620.1)	0.933 (0.814-0.976)
Remote Myocardium	-43.8 (-120.4-32.7)	0.574 (-0.106-0.836)

[a] Mean % difference between standard uptake value (SUV; kBq/mL) measurements (95% limits of agreement), and [b] ICC (intraclass correlation coefficient) values (95% confidence intervals) for 18F-fluciclatide myocardial uptake and residual blood pool activity.

SVC, superior vena cava; TBR_{mean}, mean tissue to background ratio.

Supplementary Table 3; Comparison of 18F-Fluciclatide Uptake and Indices of Infarction

	18F-Fluciclatide Infarct uptake (TBR$_{mean}$)	Δ 18F-Fluciclatide Infarct uptake (1st-2nd scan, TBR$_{mean}$)	Mean ECV (%)	Infarct Size (g/m^2)
Clinical Characteristics				
Peak hs-cTnI (ng/l)	r=0.13 (-0.31-0.54) p=0.56	r=-0.27 (-0.66-0.24) p=0.30	r=0.61 (0.23-0.82) p=0.003	r=0.59 (0.22-0.81) p=0.004
hs-CRP (mg/L)	r=-0.20 (-0.58-0.25) p=0.38	r=-0.04 (-0.54-0.48) p=0.90	r=-0.02 (-0.45-0.41) p=0.92	r=0.55 (0.16-0.80) p=0.009
Baseline CMR Assessment				
LVEF (%)	r=-0.08 (-0.49-0.36) p=0.72	r=0.03 (-0.46-0.50) p=0.91	r=-0.12 (0.53-0.32) p=0.59	r=-0.44 (-0.73--0.01) p=0.05
LV mass (g/m^2)	r=-0.19 (0.57-0.26) p=0.03	r=0.28 (-0.23-0.67) p=0.26	r=0.18 (-0.27-0.57) p=0.43	r=0.52 (0.12-0.78) p=0.01
Infarct size (g/m^2)	r=0.03 (-0.41-0.45) p=0.90	r=0.07 (-0.43-0.52) p=0.82	r=0.47 (0.06-0.75) p=0.03	-
ECV / segment (%)^{Ψ}	r=0.37 (0.28-0.45) p<0.001	r=0.22 (0.09–0.34) p=0.003	-	-
Follow-up CMR Assessment (9 months)				
Δ LVEF (%)	r =-0.23 (-0.65-0.30) p=0.39	r=-0.37 (-0.75-0.19) p=0.13	r=-0.24 (-0.66-0.28) p=0.36	r=0.12 (-0.40-0.58) p=0.66
Δ LV mass (g/m^2)	r=0.14 (-0.38-0.60) p=0.60	r=0.16 (-0.39-0.64) p=0.57	r=-0.60 (-0.85--0.16) p=0.01	r=-0.35 (-0.72-0.17) p=0.17
Δ LVEDV (mL/m^2)	r=0.34 (-0.19-0.71) p=0.20	r=-0.47 (-0.80-0.08) p=0.09	r=-0.22 (-0.64-0.31) p=0.41	r=-0.06 (-0.54-0.45) p=0.83
Δ Infarct size (g/m^2)	r=0.25 (-0.28-0.66) p=0.35	r=-0.14 (-0.62-0.41) p=0.62	r=-0.61 (-0.85-0.16) p=0.01	r=-0.42 (-0.76-0.08) p=0.10
Δ ECV / segment (%)	r=-0.11 (-0.22-0.01) p=0.07	r=-0.33 (-0.70-0.16) p=0.18	-	-

^{Ψ} ECV and PET association assessed per segment. Abbreviations: hs-cTnI, high sensitivity cardiac troponin I; hs-CRP, high sensitivity c-reactive protein; LVEF, left ventricular ejection fraction; LV, left ventricular; LVEDV, left ventricular end diastolic volume; ECV, mean extracellular volume

References

1   Mena E, Owenius R, Turkbey B, *et al.* [18F]Fluciclatide in the in vivo evaluation of human melanoma and renal tumors expressing αvβ3 and αvβ5 integrins. *Eur J Nucl Med Mol Imaging* 2014;**41**:1879–88. doi:10.1007/s00259-014-2791-x

2   Kenny LM, Coombes RC, Oulie I, *et al.* Phase I trial of the positron-emitting Arg-Gly-Asp (RGD) peptide radioligand 18F-AH111585 in breast cancer patients. *Journal of Nuclear Medicine* 2008;**49**:879–86. doi:10.2967/jnumed.107.049452

3   Tomasi G, Kenny L, Mauri F, *et al.* Quantification of receptor-ligand binding with [18F]fluciclatide in metastatic breast cancer patients. *Eur J Nucl Med Mol Imaging* 2011;**38**:2186–97. doi:10.1007/s00259-011-1907-9

4   Dweck MR, Jenkins WSA, Vesey AT, *et al.* 18F-NaF Uptake Is a Marker of Active Calcification and Disease Progression in Patients with Aortic Stenosis. *Circulation: Cardiovascular Imaging* Published Online First: 7 February 2014. doi:10.1161/CIRCIMAGING.113.001508

5   Dweck MR, Jones C, Joshi NV, *et al.* Assessment of Valvular Calcification and Inflammation by Positron Emission Tomography in Patients With Aortic Stenosis. *Circulation* 2012;**125**:76–86. doi:10.1161/CIRCULATIONAHA.111.051052

6   Cerqueira MD, Weissman NJ, Dilsizian V, *et al.* Standardized myocardial segmentation and nomenclature for tomographic imaging of the heart. A statement for healthcare professionals from the Cardiac Imaging Committee of the Council on Clinical Cardiology of the American Heart Association. 2002. 539–42.

7   Chan W, Duffy SJ, White DA, *et al.* Acute left ventricular remodeling following myocardial infarction: coupling of regional healing with remote extracellular matrix expansion. *JACC Cardiovasc Imaging* 2012;**5**:884–93. doi:10.1016/j.jcmg.2012.03.015

8   Kim RJ, Wu E, Rafael A, *et al.* The use of contrast-enhanced magnetic resonance imaging to identify reversible myocardial dysfunction. *N Engl J Med* 2000;**343**:1445–53. doi:10.1056/NEJM200011163432003

9   Treibel TA, White SK, Moon JC. Myocardial Tissue Characterization: Histological and Pathophysiological Correlation. *Curr Cardiovasc Imaging Rep* 2014;**7**:9254. doi:10.1007/s12410-013-9254-9

10 Chin CWL, Shah ASV, McAllister DA, *et al.* High-sensitivity troponin I concentrations are a marker of an advanced hypertrophic response and adverse outcomes in patients with aortic stenosis. *European Heart Journal* 2014;**35**:2312–21. doi:10.1093/eurheartj/ehu189

11 Chin CWL, Semple S, Malley T, *et al.* Optimization and comparison of myocardial

T1 techniques at 3T in patients with aortic stenosis. *Eur Heart J Cardiovasc Imaging* Published Online First: 25 November 2013. doi:10.1093/ehjci/jet245

12 Messroghli DR, Greiser A, Fröhlich M, *et al.* Optimization and validation of a fully-integrated pulse sequence for modified look-locker inversion-recovery (MOLLI) T1 mapping of the heart. *J Magn Reson Imaging* 2007;**26**:1081–6. doi:10.1002/jmri.21119

13 Shah ASV, Chin CWL, Vassiliou V, *et al.* Left ventricular hypertrophy with strain and aortic stenosis. *Circulation* 2014;**130**:1607–16. doi:10.1161/CIRCULATIONAHA.114.011085

14 Chen W, DILSIZIAN V. PET Assessment of Vascular Inflammation and Atherosclerotic Plaques: SUV or TBR? *Journal of Nuclear Medicine* 2015;**56**:503–4. doi:10.2967/jnumed.115.154385